

High-efficiency stretchable light-emitting polymers from thermally activated delayed fluorescence

Received: 21 January 2022

Accepted: 10 March 2023

Published online: 6 April 2023

 Check for updates

Wei Liu^{1,10}, Cheng Zhang^{1,10}, Riccardo Alessandri¹, Benjamin T. Diroll², Yang Li¹, Heyi Liang¹, Xiaochun Fan³, Kai Wang³, Himchan Cho^{4,8}, Youdi Liu¹, Yahao Dai¹, Qi Su¹, Nan Li¹, Songsong Li¹, Shinya Wai¹, Qiang Li⁵, Shiyang Shao^{5,9}, Lixiang Wang⁵, Jie Xu², Xiaohong Zhang^{3,6}, Dmitri V. Talapin^{1,2,4}, Juan J. de Pablo^{1,7}✉ & Sihong Wang^{1,2,7}✉

Stretchable light-emitting materials are the key components for realizing skin-like displays and optical biostimulation. All the stretchable emitters reported to date, to the best of our knowledge, have been based on electroluminescent polymers that only harness singlet excitons, limiting their theoretical quantum yield to 25%. Here we present a design concept for imparting stretchability onto electroluminescent polymers that can harness all the excitons through thermally activated delayed fluorescence, thereby reaching a near-unity theoretical quantum yield. We show that our design strategy of inserting flexible, linear units into a polymer backbone can substantially increase the mechanical stretchability without affecting the underlying electroluminescent processes. As a result, our synthesized polymer achieves a stretchability of 125%, with an external quantum efficiency of 10%. Furthermore, we demonstrate a fully stretchable organic light-emitting diode, confirming that the proposed stretchable thermally activated delayed fluorescence polymers provide a path towards simultaneously achieving desirable electroluminescent and mechanical characteristics, including high efficiency, brightness, switching speed and stretchability as well as low driving voltage.

Electroluminescent (EL) devices represent one of the central components of multiple modern technologies. They offer unique functionality for information visualization, wireless signal/power transmission and medical therapies. After decades of development,

organic light-emitting diodes (OLEDs) have become one of the most advanced EL technologies, particularly for the display industry, owing to advantages that include high efficiency, high brightness, low-voltage operation, low prices, large-area scalability and mechanical bendability.

¹Pritzker School of Molecular Engineering, The University of Chicago, Chicago, IL, USA. ²Nanoscience and Technology Division, Argonne National Laboratory, Lemont, IL, USA. ³Institute of Functional Nano & Soft Materials (FUNSOM), Joint International Research Laboratory of Carbon-Based Functional Materials and Devices, Soochow University, Suzhou, China. ⁴Department of Chemistry and James Franck Institute, The University of Chicago, Chicago, IL, USA. ⁵State Key Laboratory of Polymer Physics and Chemistry, Changchun Institute of Applied Chemistry, Chinese Academy of Sciences, Changchun, China. ⁶Jiangsu Key Laboratory of Advanced Negative Carbon Technologies, Soochow University, Suzhou, China. ⁷Center for Molecular Engineering, Argonne National Laboratory, Lemont, IL, USA. ⁸Present address: Department of Materials Science and Engineering, Korea Advanced Institute of Science and Technology (KAIST), Daejeon, Republic of Korea. ⁹Present address: State Key Laboratory of Marine Resource Utilization in South China Sea, School of Materials Science and Engineering, Hainan University, Haikou, China. ¹⁰These authors contributed equally: Wei Liu, Cheng Zhang. ✉e-mail: depablo@uchicago.edu; sihongwang@uchicago.edu

Recently, a growing desire to intimately integrate electronics with the human body in the form of wearable and implantable devices has spurred new needs for the additional development of EL devices¹, particularly along the lines of incorporating skin-like softness and stretchability. Such stretchable EL devices will find applications as on-skin displays^{2,3}, optical sensors (for example, for monitoring oxygen saturation)⁴, wearable imaging systems⁵ or implanted optical stimulation (for example, for optogenetics)⁶, to name a few. In contrast to other types of stretchable device, including sensors^{7–10} and transistors^{11–13}, stretchable EL devices have lagged behind in terms of combining high stretchability with high EL efficiency.

Initial efforts to impart stretchability to EL devices and displays were built on strain engineering designs for non-stretchable inorganic light-emitting diodes or OLEDs^{4,14–16}, which inevitably sacrifice resolution and visualization effects to achieve limited skin or tissue-like mechanical properties. A different avenue for circumventing these limitations is to impart intrinsic stretchability to EL devices. The demonstrated devices to date, however, have been based on device structures (for example, light-emitting capacitors (LECs) and light-emitting electrochemical cells (LEECs)) that are inferior to OLEDs, and/or low-efficiency emissive (that is, fluorescent) materials^{2,3,17–24}. As a result, stretchability has been attained by sacrificing some of the performance characteristics, including EL efficiency, brightness, driving voltage and switching speed. In particular, for emissive materials capable of operating under 20 V, stretchability has only been realized on polymers (mostly poly(*p*-phenylene vinylene) with the commercial name of Super Yellow (SY)) that emit only through fluorescence (FL), which stands for the rapid decay of singlet excitons), with inherently low efficiency^{20–22}. According to spin statistics^{25,26}, singlet excitons only correspond to 25% of all the excitons formed from the recombination of electrons and holes, with the majority—75%—being triplet excitons. Such FL emissive materials, which can be regarded as the first generation of organic emitters, can only achieve the maximum internal quantum efficiency of 25% (refs. 27,28), and the maximum external quantum efficiency (EQE) is, therefore, only 5% (refs. 29,30). Additional improvement in the EL performance of stretchable OLEDs is fundamentally limited by the lack of stretchable emissive materials having high-efficiency EL.

Note that the successful commercialization of OLED technologies has been largely enabled by materials innovations that realized the effective harnessing of triplet excitons for light emission, in attempts to reach near-unity internal quantum efficiency. So far, this has been primarily achieved by two types of organic emitter: phosphorescent (PH) emitters that incorporate heavy metal ions to exert strong spin-orbit coupling so as to facilitate direct triplet emissions^{31,32} (second-generation emitters), and thermally activated delayed fluorescence (TADF) emitters^{33–35} that have significantly reduced energy-level splitting (ΔE_{ST}) between singlet (S_1) and triplet (T_1) excited states, thereby enabling an efficient reverse intersystem crossing (RISC) process from T_1 to S_1 (third-generation emitters). Compared with PH emitters, heavy-metal-free TADF emitters have minimal biological/environmental toxicity and lower prices, which are desirable features for human-integrated applications. Imparting stretchability to TADF emitters, therefore, provides a particularly promising avenue for the development of high-efficiency stretchable OLEDs. So far, most of the reported TADF emitters consist of small molecules, which cannot offer stretchability and among the recently developed TADF polymers³⁶, stretchability has never been reported.

Here we introduce a molecular design strategy for stretchable TADF polymers that involves embedding soft alkyl chains between TADF units in the polymer backbone. The resulting polymers exhibit substantial stretchability, well above 100% strain, maintaining an EQE as high as ~10%, which is twice the theoretical limit (5%) of FL polymers^{29,30} used in all the reported stretchable EL devices. By combining systematic experimental characterization and atomic-level molecular

simulations of TADF polymer designs of varying alkyl chain lengths, we demonstrate that neither the soft chain design nor the stretching process has measurable deleterious effects on the EL process and efficiency. Furthermore, to assess the potential of such stretchable TADF polymers for building fully stretchable high-performance OLED devices, we created a device structure that exhibits a high EQE of 3.3%, current efficiency of 10.2 cd A⁻¹, low turn-on voltage of 4.75 V with little precedent in the literature and skin-like stretchability of 60%.

Designs of stretchable TADF polymers

It is known that introducing alkyl chains of limited length into a polymer backbone can increase molecular flexibility, thereby enhancing a polymer's softness and deformability^{37–39}. It is, therefore, reasonable to expect the insertion of soft alkyl chains between TADF units in a polymer backbone (Fig. 1a) to dissipate strain energy. Because the EL process is primarily confined to the local TADF units (Fig. 1b), we hypothesize that the presence of alkyl chains should have a minimal influence on EL performance. Furthermore, with charge transport occurring primarily through hopping between adjacent TADF units on the same or different chains, we also hypothesize that the percolation network formed by the TADF units for long-range charge hopping should not be altered by the insertion of alkyl chains below a certain length.

To systematically implement and study this general concept, we designed and synthesized a series of four polymers (labelled PDKCM, PDKCP, PDKCH and PDKCD; Fig. 1c, Supplementary Figs. 1–4 and Supplementary Table 1) that have the same TADF units, but different alkyl chain lengths of 1, 3, 6 and 10 carbons, respectively. The TADF unit consists of acridine–benzophenone as the electron donor–acceptor (D–A) pair, which has been shown to generate close-to-perpendicular dihedral angles and provide high EL efficiency^{40,41}. The alkyl chain linkage in the backbone is realized through benzo-ether capping on carbazole groups, where the TADF units are pendant as the side groups. Taking PDKCD as an example, the optimized conformational structure obtained by density functional theory (DFT) shows that the dihedral angle between the D and A groups in such a polymer is indeed close to 90° (Fig. 1d and Supplementary Figs. 5–9), which should ensure a small ΔE_{ST} value and lead to an efficient TADF process. As far as the mechanical properties are concerned, the measurements of crack-onset strain and glass transition temperature (T_g) confirm the expected trend, that is, a longer alkyl chain (of up to ten carbons) can more effectively enhance the chain dynamics and increase stretchability to over 125% strain (Fig. 1e and Supplementary Figs. 10 and 11). With our stretchable TADF polymer serving as the emitting layer (EML), high EL performance (that is, efficiency and brightness) and high stretchability are combined in fully stretchable EL devices (Fig. 1f). More generally, this avenue of TADF-OLEDs for stretchable EL devices favourably compares with previous reports based on other strategies^{18,19,22}, and provides a promising path for meeting five important performance metrics (Fig. 1g): high efficiency, switching speed, brightness and stretchability, as well as low driving voltage.

Photophysical and electroluminescence characterizations

We first investigate the influence of alkyl chains of different lengths on the photophysical behaviour through a combination of experimental characterization and theoretical calculations using DFT and atomistic molecular dynamics (MD) simulations. For comparison, we also synthesized the small-molecule TADF emitter DKC (Supplementary Fig. 3) with the same TADF unit. The four polymers and DKC exhibit two charge transfer (CT) absorption peaks: CT₂ in 350–400 nm and CT₁ in 400–450 nm (Fig. 2a and Supplementary Fig. 12), which correspond to carbazole-to-benzophenone transfer and acridine-to-benzophenone transfer, respectively⁴². This is indicative of the unchanged highest occupied molecular orbital (HOMO) and lowest unoccupied molecular orbital (LUMO) distributions and energy levels, as further verified by

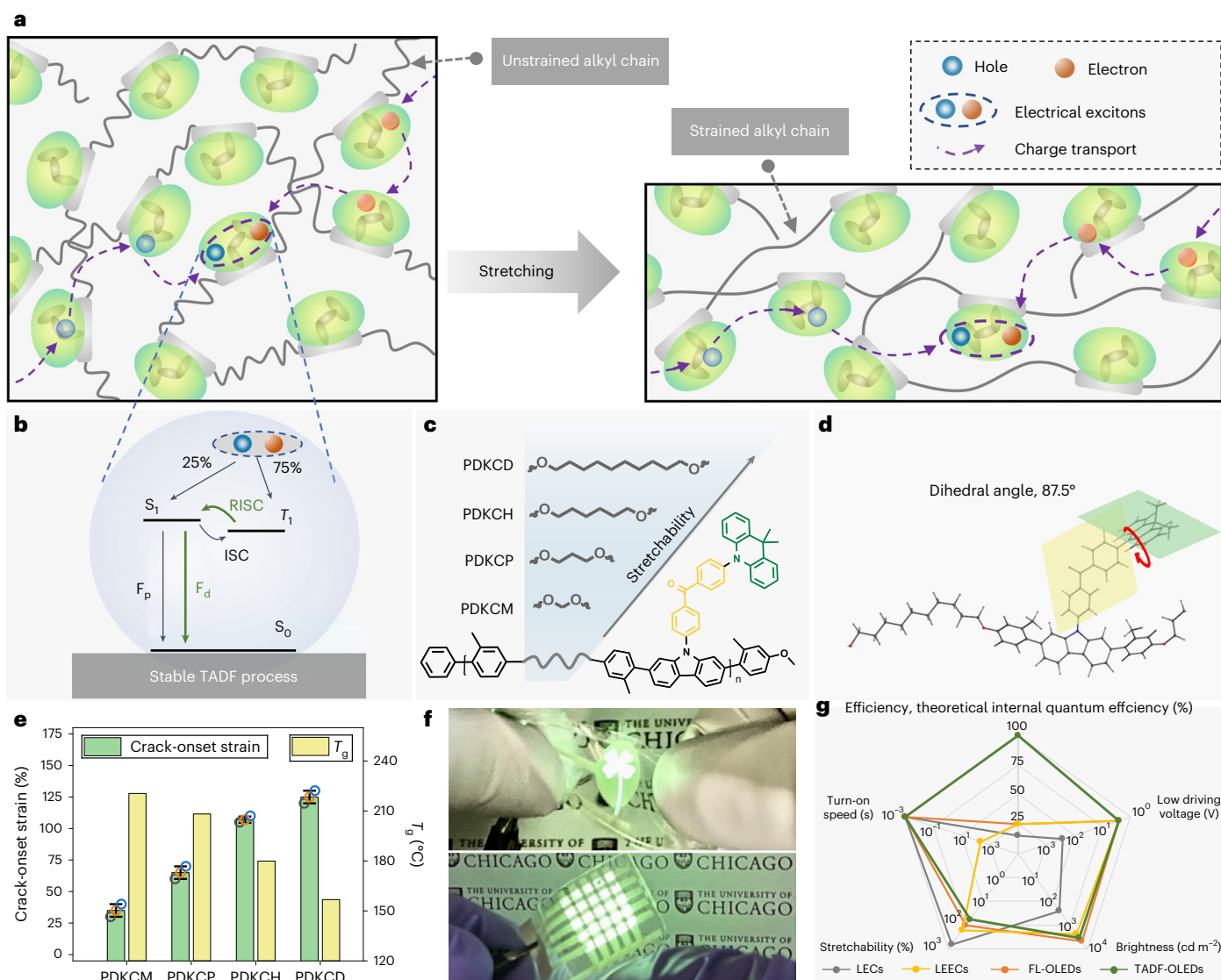


Fig. 1 | Stretchable light-emitting polymers with TADF. **a**, Design principle for realizing stretchable TADF polymers via the incorporation of soft alkyl chains into the polymer backbone. The soft alkyl chains can effectively dissipate the strain energy on stretching, keeping the TADF units unaffected. **b**, Mechanism of TADF light-emitting process in stretchable polymers. S_1 , T_1 and S_0 stand for the lowest singlet state, lowest triplet state and ground-state energy levels, respectively. ISC, RISC, F_p and F_d stand for intersystem crossing, reverse intersystem crossing, prompt fluorescence and delayed fluorescence, respectively. **c**, Chemical structures of stretchable TADF polymers having different alkyl chains in the polymer backbone. **d**, DFT simulation of the

repeating unit of the polymer PDKCD. The red-circled arrow indicates that the dihedral angle between the D and A group planes is 87.5° . **e**, T_g and crack-onset strains of stretchable TADF polymers. Data for crack-onset strains are represented as mean values \pm standard deviation (s.d.) from three samples, and the corresponding data points are overlaid. **f**, Pictures of a fully stretchable OLED and an array built with the stretchable TADF polymer PDKCD. **g**, Radar plot comparing the EL performance metrics and stretchability of the different types of stretchable EL device that have been demonstrated so far: LECs, LEECs, FL-OLEDs and TADF-emitter-based OLEDs (TADF-OLEDs), as developed in this work.

electrochemical cyclic voltammetry (Supplementary Fig. 13 and Supplementary Table 2) and DFT simulations (Fig. 2b and Supplementary Figs. 5–9). Consequently, only minimal changes are observed in the photoluminescence (PL) emission spectra (Fig. 2a and Supplementary Fig. 12) of these five emitters, all of which show one emission peak coming from CT_1 .

Next, low-temperature (77 K) FL/PH spectroscopy was performed to study the ΔE_{ST} value of TADF emitters (Fig. 2c, Supplementary Fig. 14 and Supplementary Table 3). In solution, ΔE_{ST} , which corresponds to CT_2 emission, shows a gradual decrease with increasing alkyl chain length for the four polymers. This decrease is due to the disappearance of conjugation coupling between the adjacent carbazole groups in the backbones as the alkyl chain length increases (Fig. 2b and Supplementary

Figs. 5–9). However, in the film state, with complete energy transfer from CT_2 to CT_1 (Supplementary Fig. 14b), the ΔE_{ST} values are nearly identical for all the emitters, which are small enough for an efficient TADF process. This is further verified by the D–A dihedral angle distributions from the four polymers in atomistic MD simulations (Fig. 2d). Last, the photoluminescence quantum yield (PLQY) and transient PL decay were tested to further quantify the TADF behaviour. From the transient PL decay measurement, the four TADF polymers and DKC show prompt decay at around 10 ns and delayed decay at around $3 \mu s$ (Supplementary Figs. 15 and 16), which provides direct evidence of the TADF property. The PLQY values from the four polymers remain at similar levels to that of the small-molecule TADF emitter, DKC (Fig. 2e). The extracted kinetic rate constants (Supplementary Table 4) are also

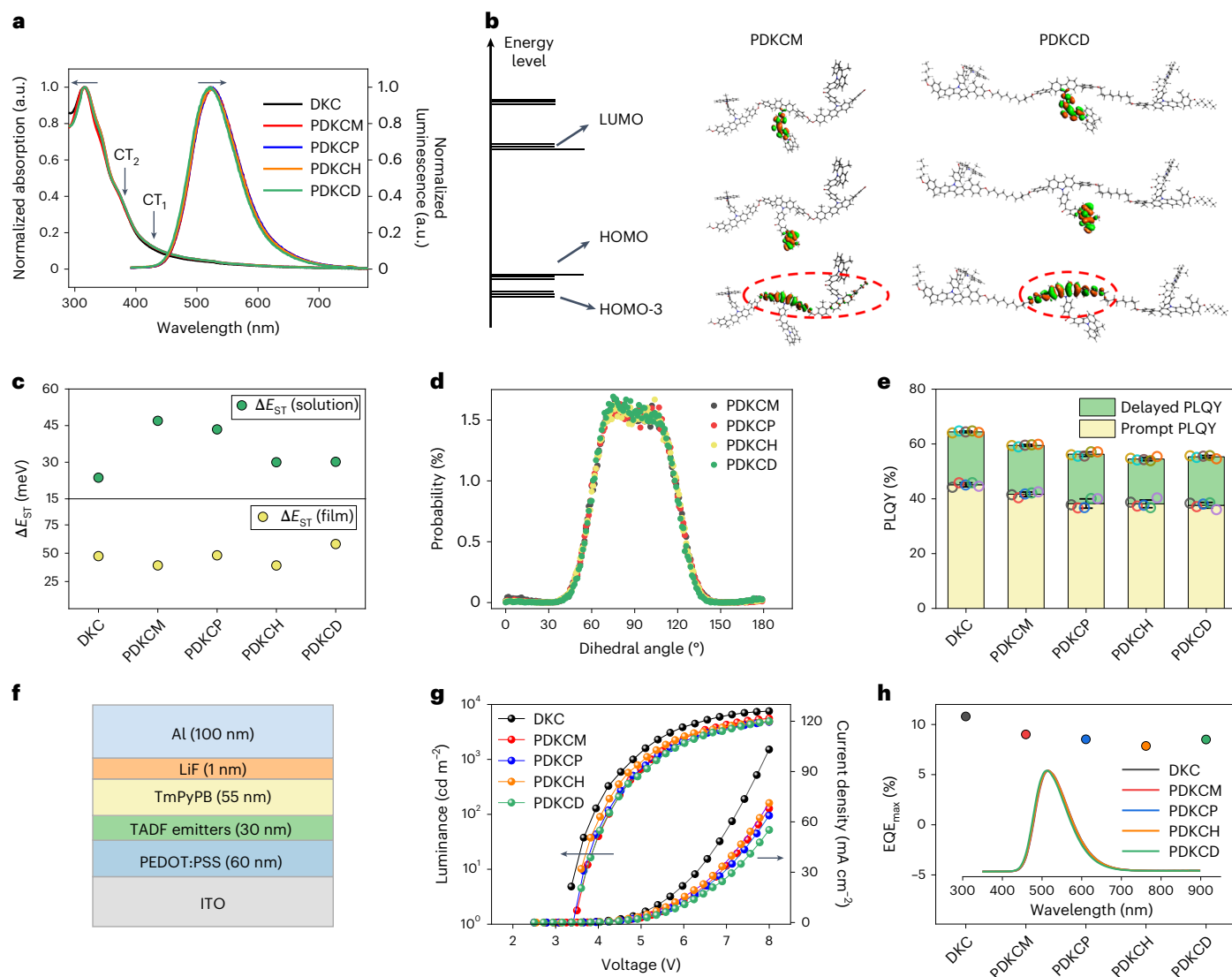


Fig. 2 | PL and EL properties of stretchable TADF polymers and corresponding small-molecule TADF emitter (DKC). **a**, Absorption spectra and room-temperature emission spectra from the thin films of the four TADF polymers and DKC. **b**, DFT-simulated LUMO, HOMO and HOMO-3 distributions in three repeating units of PDKCM and PDKCD, which reveal conjugation breaking in HOMO-3 with an increase in the alkyl linker length from one carbon to ten carbons. **c**, Values of ΔE_{ST} of stretchable TADF polymers and DKC in 2-Me-THF (10^{-3} M) and film state estimated from the onset of the FL/PH spectra at low temperatures (77 K). **d**, MD-simulated distributions of the dihedral

angle between the D and A units in the four TADF polymers. **e**, PLQY values of stretchable TADF polymers and DKC in the film state, which are separated into prompt components and delayed components. The data of prompt PLQY and delayed PLQY are represented as mean values \pm s.d. from five samples, and the corresponding data points are overlaid. **f**, Schematic of the structure of the OLED device for the characterization of EL performance of these TADF emitters in the strain-free state. TmPyPB, 1,3,5-Tri(*m*-pyridin-3-ylphenyl)benzene. **g, h**, Representative J - L - V traces (**g**), and EQE_{max} and EL spectra (inset) (**h**) of the five TADF emitters.

similar for all the emitters, which indicates the limited influence of alkyl chains on the individual steps involved in the TADF process.

We then proceed to characterize the EL properties of stretchable TADF polymers, together with DKC, as host-free EMLs in a conventional OLED structure (Fig. 2f). As shown in Fig. 2g, the four stretchable TADF polymers exhibit similar current density–voltage (J - V) and luminance–voltage (L - V) traces. Compared with DKC, there is only a minor decrease in the maximum luminance, which might be due to the different packing structures of TADF units in polymer chains versus small molecules. The EL spectra (Fig. 2h, inset) are also similar. Furthermore, the comparable EL performance of the polymers and DKC emitter is also evident in the efficiency, with our stretchable TADF polymers achieving a total maximum EQE (EQE_{max}) value of ~10% (Fig. 2h). Such performance is well within the typical range of the

reported non-stretchable TADF polymers as host-free emitters (Supplementary Table 5 and Supplementary Figs. 17 and 18). These results clearly show that the soft alkyl chain design introduced here to achieve stretchability does not affect the EL performance.

Mechanical and photophysical behaviours under stretching

The stretchability of the four TADF polymer films was tested by measuring the stretching-induced evolution of the luminescent performance up to 100% strain. Consistent with the mechanical properties (Fig. 1e), the crack sizes and densities under large strains between 50% and 100% (Fig. 3a and Extended Data Fig. 1) are greatly reduced as the alkyl chain length is increased. Importantly, the PDKCD film under 100% strain shows a morphology that remains intact, without any cracks even at

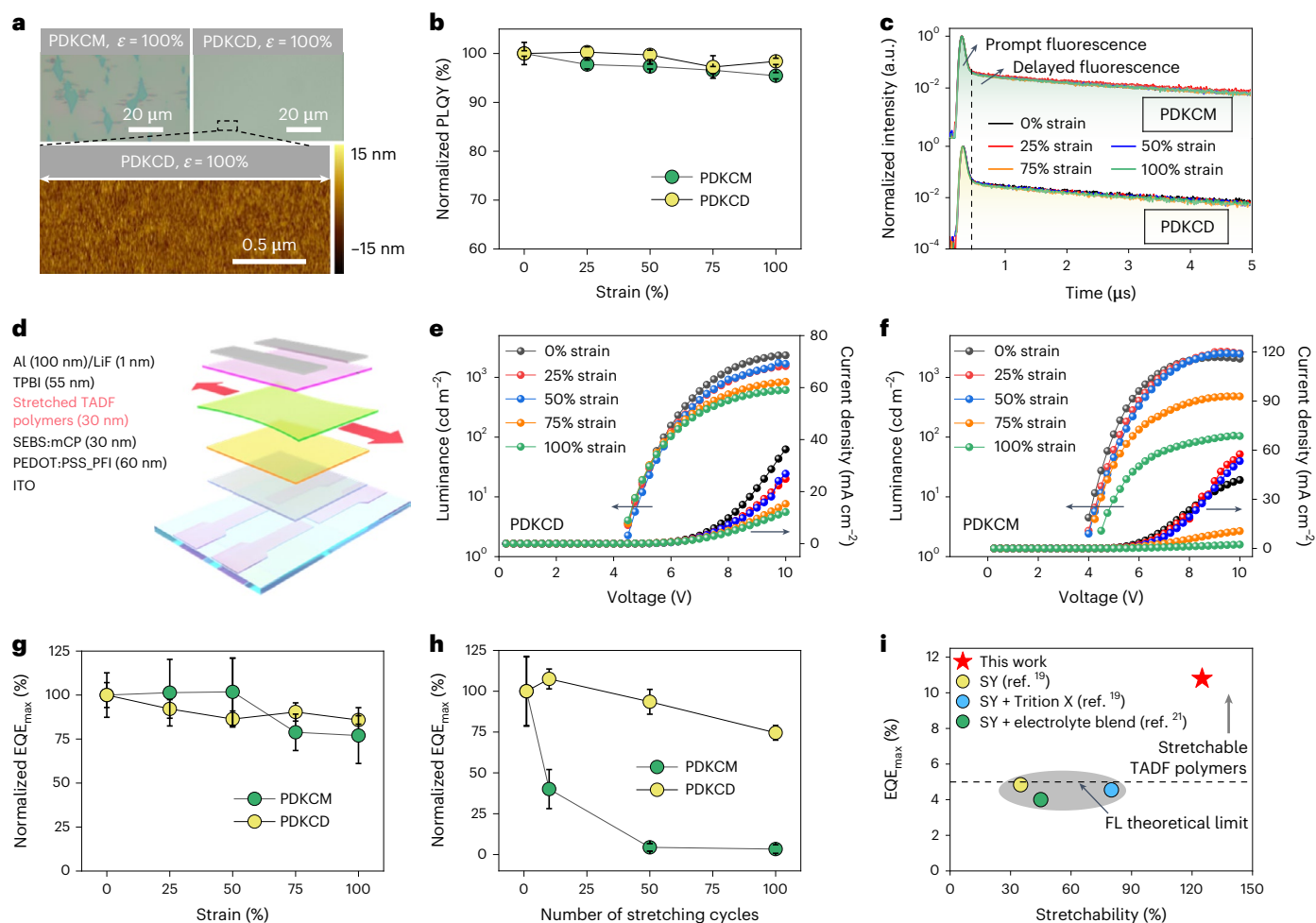


Fig. 3 | PL and EL properties of stretchable TADF polymers under stretching.

a, Optical microscopy images of PDKCM and PDKCD thin films under 100% strain, with the AFM height image as the nanoscale view of the PDKCD film. **b**, Normalized PLQY values of PDKCM and PDKCD under different strains. The data of PLQY values are represented as mean values \pm s.d. from five samples. **c**, PL transient decays of PDKCM and PDKCD under different strains. **d**, Schematic of the OLED device structure for characterizing the EL performance of the stretchable TADF polymers under strain. Note that a layer of SEBS and mCP blend with a weight ratio of 1:1 (Supplementary Fig. 21) was added on top of the PEDOT:PSS/PFI hole transporting layer to facilitate the lamination of the TADF polymer films. SEBS, polystyrene-*block*-poly(ethylene-ranbutylene)-*block*-polystyrene; mCP, 1,3-bis(*N*-carbazolyl)benzene; TPBI,

2,2',2''-(1,3,5-benzinetriyl)-tris(1-phenyl-1-*H*-benzimidazole). **e**, Representative *J*-*V* and *L*-*V* traces of OLEDs with PDKCD under different strains.

f, Representative *J*-*V* and *L*-*V* traces of OLEDs with PDKCM under different strains. **g**, Normalized EQE_{max} from PDKCD and PDKCM under different strains. EQE data are represented as mean values \pm s.d. from three devices. **h**, Normalized EQE_{max} from PDKCD and PDKCM under 100 repeated stretching cycles to 100% strain. EQE data are represented as mean values \pm s.d. from three devices. **i**, Comparison of EQE_{max} and stretchability given by PDKCD (this work) with the corresponding values obtained from previously reported stretchable light-emitting polymers based on FL emitters (for example, SY); the dashed line represents the theoretical limit for the EQE of any FL polymer.

nanoscale dimensions (Fig. 3a and Supplementary Fig. 19). The impacts of strain and crack formation were first evaluated on the PL properties. Since PL is essentially a local process occurring at the TADF units, the strain has little influence on either the PLQY values (Fig. 3b and Supplementary Fig. 20) or the transient PL decay behaviours (Fig. 3c and Supplementary Figs. 15 and 16) in all the polymers proposed here, even when crack formation occurs.

Furthermore, for studying the polymers' intrinsic EL performance under stretching, OLED devices with a conventional device structure (Fig. 3d and Supplementary Fig. 21) were assembled by physically transferring the stretched TADF polymer films onto a rigid device stack. The measured OLED performance (Supplementary Figs. 22 and 23) indicates that the stretching stabilities of the EL performance of these four TADF polymer films follow the same trends as their mechanical stretchability. In particular, the PDKCD film (Fig. 3e) provides much more stable luminance and current density during stretching of up to 100% strain than the PDKCM (Fig. 3f) film. The decrease in both current

and luminance of PDKCM with strain is probably due to the negative influence of crack formation in the EML, which could be suffering from the combined effects of contact deterioration between the cracked emitter and adjacent electron/hole transporting layers, as well as the increase in crack-induced charge trapping. The extracted EQE_{max} values (Fig. 3g) from the PDKCD film exhibit a negligible decrease during stretching of up to 100% strain, and remain at the original level of 10%. After repeated stretching to 100% strain for 100 cycles (Fig. 3h), PDKCD exhibits a much more stable performance than PDKCM. Taken together, the results outlined above indicate that compared with the reported stretchable light-emitting polymers^{19,21,43} (all of which are based on the first-generation FL emitters (for example, SY)), our stretchable TADF polymers exhibit substantial improvements in both EL efficiency (as represented by EQE_{max}), which is twice the theoretical limit of FL emitters, and stretchability (based on the crack-onset strain) (Fig. 3i). Furthermore, as shown in Supplementary Figs. 24 and 25, the generalizability of our strategy to different types of TADF structure has

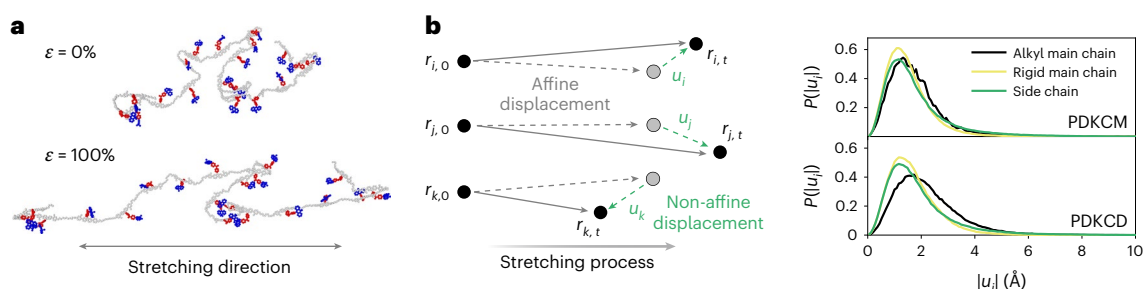


Fig. 4 | MD simulations of stretchable TADF polymers under stretching. **a**, Snapshots of one representative chain taken from an MD simulation of PDKCD at 0% and 100% strain. Backbone is rendered in grey; D, blue; A, red. The full polymer assembly is shown in Extended Data Fig. 4. **b**, Schematic of non-affine

displacements (left). Non-affine displacement distributions for the alkyl main chains, rigid main chains and side chains at 5% strain for polymers PDKCM and PDKCD (right).

also allowed us to impart stretchability onto two other TADF designs that give blue- and red-colour emissions, respectively.

In-depth study of strain dissipation process using MD simulations

Atomistic MD simulations were performed to gain molecular-level insights into the mechanism for strain dissipation and its correlation with the underlying EL processes (Supplementary Figs. 26–33 and Extended Data Figs. 4 and 5). First, by tracking the conformation of polymer chains in our model PDKCD film, we observe that stretching causes polymer molecules to gradually orient in the direction of deformation (Fig. 4a), thereby providing a mechanism for strain dissipation. At a more local level, we have examined the non-affine displacement⁴⁴ field to show that the long alkyl units inserted into the backbone are major contributors to strain dissipation. Note that non-affine displacements have been particularly useful in the context of glassy materials to understand the origin of activated processes and dynamic heterogeneities⁴⁴. Specifically, by separately tracking the distributions of the non-affine displacement of conjugated and alkyl segments in the main chain and TADF D–A segments on the side chains of the four polymers (Fig. 4b and Extended Data Fig. 5), we find that non-affine displacements monotonically increase with the alkyl chain length. A comparison of the alkyl non-affine displacement field in PDKCM and PDKCD reveals that in the former, all the atoms undergo comparable non-affine displacements. In PDKCD, the alkyl segments undergo much larger non-affine displacements during deformation. These results indicate that even well within the glassy state, the alkyl segments of PDKCD act as compliant domains capable of absorbing much of the energy that is accrued during stretching, thereby delaying the onset of crack formation. Note that past reports of ‘soft’ and ‘hard’ hot spots in glasses have been limited to homopolymers^{45,46} or small-molecule glasses^{47,48}. There is no precedent for the observation of ‘designer’ compliant domains within a polymeric backbone, and the findings reported could provide a fruitful platform for the development of toughened polymeric glasses. To further reveal such differences from another angle, we also tracked the evolution of distances between the terminal atoms of individual alkyl units and TADF segments during stretching of up to 100% strain (Supplementary Fig. 27). We observed that the ten-carbon alkyl units in PDKCD are elongated rather effectively by the applied strain, whereas the TADF units and the one-carbon alkyl units in PDKCM exhibit little conformational changes that would contribute to strain dissipation. In an attempt to extend our understanding of the strain’s influence on TADF behaviour and charge transport, we also analysed the intramolecular conformational and intermolecular packing structures of the TADF segments in these four polymers both at rest and during stretching. First, we find that within the statistical uncertainty of our calculations, the D–A dihedral angle distributions of the TADF units in all the four polymers remain almost unchanged

under strain (Supplementary Fig. 28). Second, the correlation of the distances and angles between the first nearest D–D pairs and A–A pairs and the second-nearest D–A pairs exhibit minor changes during the stretching process (Supplementary Figs. 29–31). The robustness of the TADF packing structure is confirmed by the radial distribution function of D and A units (Supplementary Figs. 32 and 33). These results serve to further support the view that both alkyl units and applied strain before crack formation have a limited influence on the underlying long-range charge-carrier hopping processes and help explain our experimental observations pertaining to the EL performance of these polymers.

Fully stretchable TADF-OLEDs

Here we utilize our most stretchable TADF polymer, PDKCD, to realize fully stretchable high-performance OLEDs. The device structure (Fig. 5a) combines a set of material choices (Supplementary Figs. 34–39 and Extended Data Figs. 6–9) that not only achieve stretchability^{49,50} for each layer but also provide the desired energy level alignment (Fig. 5b) for charge injection. The resulting fully stretchable OLED achieves a low turn-on voltage of 4.75 V and therefore can be powered by a commercial battery (Fig. 5c). The fast switching speed (Supplementary Fig. 40) of the device opens the door to potential applications in displays (with a typical operating frequency of 120 Hz). The EL performance (Fig. 5d) of the device at the initial state with 0% strain corresponds to a record-high EQE_{max} of 3.3% (by adding together the emission from the cathode and anode sides; Fig. 5e) compared with previously reported stretchable OLEDs (Supplementary Table 6). Compared with PDKCD’s EL performance in rigid OLED devices, the lower EQE observed in the fully stretchable OLEDs should primarily arise from the silver nanowire (AgNW) electrodes’ relatively low conductance (Extended Data Fig. 6), limited transparency and non-ideal energy level alignment for electron injection.

As a result of the high stretchability of PDKCD, as well as all the other layers, the device introduced above can be stretched to 60% strain, maintaining an unshifted luminescent wavelength with the CIE coordinates of (0.31, 0.53) (Fig. 5f). Both EQE_{max} (Fig. 5g) and luminance (Fig. 5g,h and Supplementary Fig. 41) remain above 50% and 60% of their original values, respectively. The observed decrease in EL performance under stretching is mainly attributed to the increase in resistance of the AgNW electrodes (Extended Data Fig. 6), as well as the deterioration in interface contacts. When stretched to over 60% strain, device failure is primarily due to the shorting between AgNW electrodes. Note that we have also demonstrated a 5 × 5 array (Fig. 1f), serving to underscore the potential for future display applications. Moving forward, it will be important to introduce improvements to the stretchable electrodes and interfaces for more efficient charge injection, better mechanical stability and light outcoupling, thereby providing considerable room for the improvement in EL performance and stretchability in fully stretchable TADF-OLEDs. For future applications

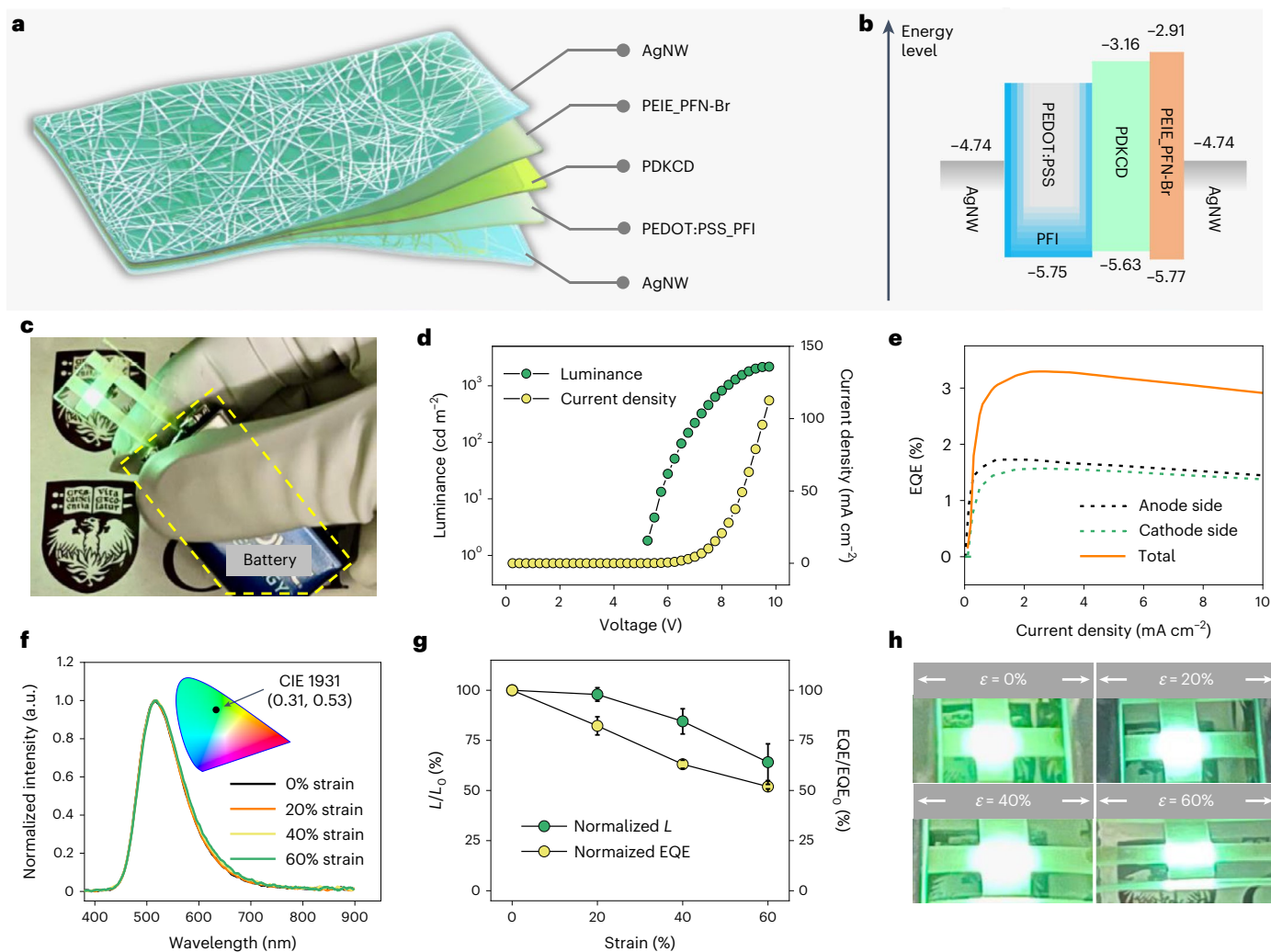


Fig. 5 | Fully stretchable OLEDs fabricated with PDKCD. **a**, Schematic of the device structure. PEIE and PFI are used in hole and electron injection layers, respectively, to both tune the work function of the AgNW electrodes and enable layer stretchability (Extended Data Figs. 7–9 and Supplementary Figs. 35–38). PFN-Br, poly[(9,9-bis(3'-(*N,N*-dimethyl)-*N*-ethylammonium)-propyl)-2,7-fluorene)-*alt*-2,7-(9,9-dioctylfluorene)]; PEIE, polyethyleneimine ethoxylated; PFI, perfluorinated ionomers. **b**, Energy-level diagram of the device. **c**, Photograph showing the stretchable OLED lit up by a battery. **d–f**, EL performance of a stretchable OLED under pristine conduction: J – V – L curves (**d**); EQE– J traces

measured from both anode and cathode sides of the OLED, with the solid line showing the total EQE combining the emission from both sides (**e**); EL spectra and CIE chromaticity diagram (inset) marked with the emission coordinates of the stretchable OLED under different strains (**f**). **g**, Normalized luminance intensity (L/L_0) and EQE (EQE/EQE_0) of the stretchable OLED at different strains. The data of L/L_0 and EQE/EQE_0 are represented as mean values \pm s.d. from three devices. **h**, Photographs of a representative OLED device stretched from 0% to 20%, 40% and 60% strains.

of our fully stretchable OLEDs, it would also be highly desirable to develop an encapsulating film having moisture/gas barrier properties, high stretchability, high transparency and compatible interfaces with other device layers.

Outlook

Through the design and synthesis of new polymers comprising linear alkyl linkers and TADF units, we have imparted stretchability onto a light-emitting polymer that can break the 5% EQE limit only from singlet emission, thereby achieving a record EL efficiency for intrinsically stretchable emitters. Our systematic experimental characterization and computational simulations show that longer alkyl linkers (in the range of ten carbon units) provide more effective strain dissipation capabilities than short linkers and thus higher stretchability, without sacrificing EL performance. As demonstrated in the fully stretchable OLED devices presented here, we anticipate that the successful development of stretchable TADF polymers

offers considerable potential for applications and a technologically feasible path for stretchable optoelectronic devices for use in human-interactive applications.

Online content

Any methods, additional references, Nature Portfolio reporting summaries, source data, extended data, supplementary information, acknowledgements, peer review information; details of author contributions and competing interests; and statements of data and code availability are available at <https://doi.org/10.1038/s41563-023-01529-w>.

References

1. Won, S. M., Song, E., Reeder, J. T. & Rogers, J. A. Emerging modalities and implantable technologies for neuromodulation. *Cell* **181**, 115–135 (2020).
2. Shi, X. et al. Large-area display textiles integrated with functional systems. *Nature* **591**, 240–245 (2021).

3. Son, D. et al. An integrated self-healable electronic skin system fabricated via dynamic reconstruction of a nanostructured conducting network. *Nat. Nanotechnol.* **13**, 1057–1065 (2018).
4. Kim, R. H. et al. Waterproof AllnGaP optoelectronics on stretchable substrates with applications in biomedicine and robotics. *Nat. Mater.* **9**, 929–937 (2010).
5. Kim, E. H. et al. Organic light emitting board for dynamic interactive display. *Nat. Commun.* **8**, 14964 (2017).
6. Mickle, A. D. et al. A wireless closed-loop system for optogenetic peripheral neuromodulation. *Nature* **565**, 361–365 (2019).
7. You, I. et al. Artificial multimodal receptors based on ion relaxation dynamics. *Science* **370**, 961–965 (2020).
8. Jung, D. et al. Highly conductive and elastic nanomembrane for skin electronics. *Science* **373**, 1022–1026 (2021).
9. Lee, S. et al. Nanomesh pressure sensor for monitoring finger manipulation without sensory interference. *Science* **370**, 966–970 (2020).
10. Jeong, H. et al. Miniaturized wireless, skin-integrated sensor networks for quantifying full-body movement behaviors and vital signs in infants. *Proc. Natl Acad. Sci. USA* **118**, e2104925118 (2021).
11. Wang, S. W. et al. Skin electronics from scalable fabrication of an intrinsically stretchable transistor array. *Nature* **555**, 83–88 (2018).
12. Zheng, Y. Q. et al. Monolithic optical microlithography of high-density elastic circuits. *Science* **373**, 88–94 (2021).
13. Xu, J. et al. Highly stretchable polymer semiconductor films through the nanoconfinement effect. *Science* **355**, 59–64 (2017).
14. Sekitani, T. et al. Stretchable active-matrix organic light-emitting diode display using printable elastic conductors. *Nat. Mater.* **8**, 494–499 (2009).
15. White, M. S. et al. Ultrathin, highly flexible and stretchable PLEDs. *Nat. Photon.* **7**, 811–817 (2013).
16. Li, Y. F. et al. Stretchable organometal-halide-perovskite quantum-dot light-emitting diodes. *Adv. Mater.* **31**, 1807516 (2019).
17. Tan, Y. J. et al. A transparent, self-healing and high- κ dielectric for low-field-emission stretchable optoelectronics. *Nat. Mater.* **19**, 182–188 (2020).
18. Larson, C. et al. Highly stretchable electroluminescent skin for optical signaling and tactile sensing. *Science* **351**, 1071–1074 (2016).
19. Liang, J. J., Li, L., Niu, X. F., Yu, Z. B. & Pei, Q. B. Elastomeric polymer light-emitting devices and displays. *Nat. Photon.* **7**, 817–824 (2013).
20. Gao, H., Chen, S., Liang, J. & Pei, Q. Elastomeric light emitting polymer enhanced by interpenetrating networks. *ACS Appl. Mater. Interfaces* **8**, 32504–32511 (2016).
21. Kim, J. H. & Park, J. W. Intrinsically stretchable organic light-emitting diodes. *Sci. Adv.* **7**, eabd9715 (2021).
22. Liang, J. J. et al. Silver nanowire percolation network soldered with graphene oxide at room temperature and its application for fully stretchable polymer light-emitting diodes. *ACS Nano* **8**, 1590–1600 (2014).
23. Yu, Z., Niu, X., Liu, Z. & Pei, Q. Intrinsically stretchable polymer light-emitting devices using carbon nanotube-polymer composite electrodes. *Adv. Mater.* **23**, 3989–3994 (2011).
24. Zhang, Z. et al. High-brightness all-polymer stretchable LED with charge-trapping dilution. *Nature* **603**, 624–630 (2022).
25. Rothberg, L. J. & Lovinger, A. J. Status of and prospects for organic electroluminescence. *J. Mater. Res.* **11**, 3174–3187 (1996).
26. Tsutsui, T. & Saito, S. *Organic Multilayer-Dye Electroluminescent Diodes—Is There Any Difference with Polymer LED?* 123–134 (Kluwer, 1993).
27. Segal, M., Baldo, M. A., Holmes, R. J., Forrest, S. R. & Soos, Z. G. Excitonic singlet-triplet ratios in molecular and polymeric organic materials. *Phys. Rev. B* **68**, 075211 (2003).
28. Wilson, J. S. et al. Spin-dependent exciton formation in π -conjugated compounds. *Nature* **413**, 828–831 (2001).
29. Patel, N., Cina, S. & Burroughes, J. High-efficiency organic light-emitting diodes. *IEEE J. Sel. Topics Quantum Electron.* **8**, 346–361 (2002).
30. Saleh, B. E. & Teich, M. C. *Fundamentals of Photonics* (Wiley, 1991).
31. Baldo, M. A. et al. Highly efficient phosphorescent emission from organic electroluminescent devices. *Nature* **395**, 151–154 (1998).
32. Lee, J. et al. Deep blue phosphorescent organic light-emitting diodes with very high brightness and efficiency. *Nat. Mater.* **15**, 92–98 (2016).
33. Di, D. et al. High-performance light-emitting diodes based on carbene-metal-amides. *Science* **356**, 159–163 (2017).
34. Hamze, R. et al. Eliminating nonradiative decay in Cu(I) emitters: >99% quantum efficiency and microsecond lifetime. *Science* **363**, 601–606 (2019).
35. Uoyama, H., Goushi, K., Shizu, K., Nomura, H. & Adachi, C. Highly efficient organic light-emitting diodes from delayed fluorescence. *Nature* **492**, 234–238 (2012).
36. Nikolaenko, A. E., Cass, M., Bourcet, F., Mohamad, D. & Roberts, M. Thermally activated delayed fluorescence in polymers: a new route toward highly efficient solution processable OLEDs. *Adv. Mater.* **27**, 7236–7240 (2015).
37. Mun, J. et al. Effect of nonconjugated spacers on mechanical properties of semiconducting polymers for stretchable transistors. *Adv. Funct. Mater.* **28**, 1804222 (2018).
38. Müller, C. et al. Tough, semiconducting polyethylene-poly(3-hexylthiophene) diblock copolymers. *Adv. Funct. Mater.* **17**, 2674–2679 (2007).
39. Oh, J. Y. et al. Intrinsically stretchable and healable semiconducting polymer for organic transistors. *Nature* **539**, 411–415 (2016).
40. Huang, J. et al. Highly efficient nondoped OLEDs with negligible efficiency roll-off fabricated from aggregation-induced delayed fluorescence luminogens. *Angew. Chem. Int. Ed.* **56**, 12971–12976 (2017).
41. Rao, J. et al. Bridging small molecules to conjugated polymers: efficient thermally activated delayed fluorescence with a methyl-substituted phenylene linker. *Angew. Chem. Int. Ed.* **59**, 1320–1326 (2020).
42. Ma, F. et al. Molecular engineering of thermally activated delayed fluorescence emitters with aggregation-induced emission via introducing intramolecular hydrogen-bonding interactions for efficient solution-processed nondoped OLEDs. *ACS Appl. Mater. Interfaces* **12**, 1179–1189 (2020).
43. Ni, M. et al. Intrinsically stretchable and stable ultra-deep-blue fluorene-based polymer with a high emission efficiency of $\approx 90\%$ for polymer light-emitting devices with a CIE_y = 0.06. *Adv. Funct. Mater.* **31**, 2106564 (2021).
44. Papakonstantopoulos, G. J., Riggleman, R. A., Barrat, J.-L. & de Pablo, J. J. Molecular plasticity of polymeric glasses in the elastic regime. *Phys. Rev. E* **77**, 041502 (2008).
45. Yoshimoto, K., Jain, T. S., Van Workum, K., Nealey, P. F. & de Pablo, J. J. Mechanical heterogeneities in model polymer glasses at small length scales. *Phys. Rev. Lett.* **93**, 175501 (2004).
46. Richard, D. et al. Predicting plasticity in disordered solids from structural indicators. *Phys. Rev. Mater.* **4**, 113609 (2020).
47. Barrat, J.-L. & de Pablo, J. J. Modeling deformation and flow of disordered materials. *MRS Bull.* **32**, 941–944 (2007).
48. Shang, B., Rottler, J., Guan, P. & Barrat, J.-L. Local versus global stretched mechanical response in a supercooled liquid near the glass transition. *Phys. Rev. Lett.* **122**, 105501 (2019).
49. Ohisa, S. et al. Conjugated polyelectrolyte blend with polyethyleneimine ethoxylated for thickness-insensitive electron injection layers in organic light-emitting devices. *ACS Appl. Mater. Interfaces* **10**, 17318–17326 (2018).

50. Jeong, S.-H. et al. Universal high work function flexible anode for simplified ITO-free organic and perovskite light-emitting diodes with ultra-high efficiency. *NPG Asia Mater.* **9**, e411 (2017).

Publisher's note Springer Nature remains neutral with regard to jurisdictional claims in published maps and institutional affiliations.

Springer Nature or its licensor (e.g. a society or other partner) holds exclusive rights to this article under a publishing agreement with the author(s) or other rightsholder(s); author self-archiving of the accepted manuscript version of this article is solely governed by the terms of such publishing agreement and applicable law.

© The Author(s), under exclusive licence to Springer Nature Limited 2023, corrected publication 2023

Methods

Materials

(4-Bromophenyl)(4-fluorophenyl)methanone and 2,7-dibromo-9H-carbazole were purchased from Combi-Blocks. 9,9-Dimethyl-9,10-dihydroacridine was purchased from Oakwood Products. 2,2',2''-(1,3,5-Benzinetriyl)-Tris(1-phenyl-1H-benzimidazole), 1,3,5-tri(*m*-pyridin-3-ylphenyl)benzene, 1,3-bis(*N*-carbazolyl)benzene (mCP) and lithium fluoride (LiF) were purchased from Xi'an Polymer Light Technology. Poly[(9,9-bis(3'-(*N,N*-dimethyl)-*N*-ethylammonium-propyl)-2,7-fluorene)-*alt*-2,7-(9,9-dioctylfluorene)] (PFN-Br) was purchased from 1-Material. Polyethylenimine, 80% ethoxylated solution (PEIE) and Nafion perfluorinated resin (PFI) solution (527084-25 ml, 5 wt% in a mixture of lower aliphatic alcohols and water) were purchased from Sigma-Aldrich and used without changing the concentration, unless mentioned. PEDOT:PSS solution (Clevios P VP CH 8000, 2.4–3.0 wt% in water) was purchased from Heraeus Deutschland and used without changing the concentration, unless mentioned. SEBS HI221 with a volume fraction of poly(ethylene-*co*-butylene) = 88% was provided by Asahi Kasei. Dow Corning SYLGARD 184 silicone elastomer clear kit was used to prepare polydimethylsiloxane (PDMS) with different base/crosslinker mix ratios for use. Thermoplastic polyurethane (TPU; Elastollan 1185 A) was provided by BASF. AgNWs (AW045) as suspensions in water were purchased from Zhejiang Kechuang Advanced Materials. Patterned indium tin oxide (ITO) glass substrates were purchased from Ossila. Other general reagents and solvents were purchased from Sigma-Aldrich or Fisher Scientific. CBM-DMAC ((4-(3,6-di-*tert*-butyl-9H-carbazol-9-yl)phenyl)(4-(9,9-dimethylacridin-10(9H)-yl)phenyl)methanone), PNB-TAC-TRZ-5 (ref. 51) and P-Ac95-TRZ05 (ref. 52) are synthesized according to the reported procedures.

Synthesis

Synthesis details of the stretchable TADF polymers can be found in the Supplementary Information.

General characterization

Number-averaged molecular weight, weight-averaged molecular weight and polydispersity index were evaluated by a Wyatt Dawn HELEOS II multi-angle light scattering instrument. Absorption was measured using a Shimadzu UV-3600 Plus ultraviolet–visible–near-infrared spectrophotometer. The PL spectra were measured with a Horiba spectrofluorometer Fluorolog 3 instrument. The FL and phosphorescence spectra were measured at 77 K using a Hitachi F-4600 fluorescence spectrometer. The measurement of the phosphorescence spectra was delayed by a chopper with a chopping speed of 40 Hz, corresponding to a delay time of ~6.25 ms. Time-resolved emission experiments were performed on samples loaded in a nitrogen cryostat that was evacuated. Time-resolved emission was performed by exciting the sample with ultraviolet pulses prepared by directing the output of a 35 fs Ti:sapphire laser into an optical parametric amplifier, with emission monitored using a streak camera. The TA Instruments Discovery 2500 differential scanning calorimeter was used to measure the glass transition temperature (T_g). Cyclic voltammetry was performed on a MultiPalmSens4 electrochemical analyser with 0.1 M *tetra-n*-butylammonium hexafluorophosphate as a supporting electrolyte, a saturated calomel electrode as a reference electrode, a platinum disk as a working electrode and a scan rate of 50 mV s⁻¹. The oxidation potential of the saturated calomel electrode relative to the vacuum level was calibrated to be 4.662 V in dimethylformamide. The cyclic voltammetry data for DKC were measured in a dimethylformamide solution, and the cyclic voltammetry data for stretchable TADF polymers are measured using films, deposited on a glassy carbon electrode, in a dimethylformamide solution. The PLQY measurements were done using an LSM Series high-power light-emitting diode (310 nm, Ocean Optics) as the light source and a fibre integration sphere (FOIS-1)

coupled with a QE Pro spectrometer (Ocean Optics) as the spectrometer. The samples were held on a home-made stage to enable the light source excited on the samples, and the emitted light was collected with the integration sphere. The Raman spectra were measured on the LabRAM HR Evo confocal Raman microscope. The transparency of the AgNW-based electrode was measured using standard visible–near-infrared light source (HL-3P-INT-CAL plus, Ocean Optics) as the light source and a fibre integration sphere (FOIS-1) coupled with a QE Pro spectrometer (Ocean Optics) as the spectrometer. All the X-ray photoemission spectroscopy (XPS) and ultraviolet photoemission spectroscopy (UPS) measurements were conducted on a Thermo Scientific K-Alpha XPS instrument with a built-in automated calibration system and an average base pressure of 10⁻⁸ T at NUANCE, Northwestern University. The XPS data were collected with monochromatic Al K α radiation. The He I (21.22 eV) radiation line from a discharge lamp was used for the UPS measurements. All the UPS measurements were done using standard procedures with a -5 V bias applied to the sample.

Simulation

The Gaussian09 (ref. 53) package was used to perform the DFT calculations with the B3LYP functional and 6-31G(d,p) basis set. The MD simulations were performed with GROMACS⁵⁴ and LAMMPS⁵⁵ packages. The visualization packages OVITO⁵⁶ and Avogadro⁵⁷ were used for all the visualizations. Simulation initialization was performed using PACKMOL^{58,59} and custom Python 3.8.5 scripts; post-processing was performed using custom Python scripts.

Surface treatment for the substrates (Si wafer, glass or quartz)

Octadecyltrimethoxysilane (OTS)-functionalized substrates were prepared following a previous method⁶⁰. Briefly, a pre-cleaned substrate was treated by O₂ plasma (150 W) for 2 min, and the OTS solution (1 μ l ml⁻¹ in trichloroethylene) was spin coated on the substrate at 0 rpm for 30 s and 3,000 rpm for 30 s. Next, the substrate was annealed in ammonium hydroxide vapour overnight to form a monolayer of OTS and then sonicated in toluene for 5 min. Finally, the substrate was cleaned and dried for use. The 3-(trimethoxysilyl)propyl methacrylate (MPTS)-functionalized substrate was prepared with a similar process to OTS functionalization, except for an additional step of crosslinking MPTS at 150 °C for 30 min before use. For the SEBS-coated substrates, the SEBS solution (8 mg ml⁻¹ in toluene) was spin coated at 3,000 rpm for 30 s, followed by annealing at 80 °C for 10 min.

Characterization of stretchable TADF polymer thin films

The thin films of our stretchable TADF polymers were prepared through the spin coating of the polymer solutions in chlorobenzene (CB) with a concentration of 8 mg ml⁻¹, on MPTS-modified Si substrates (MPTS-Si) at 1,000 rpm, followed by annealing at 120 °C for 20 min. This leads to film thicknesses of around 50 nm. The films were transferred to PDMS stamps to apply different strains and then transferred to SEBS-coated Si substrates for characterizations. The PNB-TAC-TRZ-5 and P-Ac95-TRZ05 films cannot be transferred to the PDMS stamp from MPTS-Si; instead, OTS-Si was used as the substrate for spin coating. The other parameters for making the films are the same as our stretchable polymers. For the PLQY measurement, the films were transferred to SEBS-coated quartz substrates.

Fabrication and testing of conventional rigid OLEDs

The ITO-coated glasses were first cleaned with 1 vol% Hellmanex solution, isopropyl alcohol (IPA) and deionized water, and then dried and further treated with O₂ plasma (150 W, 10 min). A PEDOT:PSS dispersion was spin coated onto ITO substrates at 4,500 rpm for 1 min as the hole injection layer/hole transporting layer, followed by annealing at 150 °C for 30 min. Then, TADF EMLs were spin coated in a glovebox from the polymer solutions of 8 mg ml⁻¹ in CB or DKC solutions of 10 mg ml⁻¹ in chloroform. The spin-coating condition is 2,000 rpm for 30 s, which

is followed by annealing at 120 °C for 30 min. Next, thermal evaporations were carried out to sequentially deposit 1,3,5-tri(*m*-pyridin-3-ylphenyl)benzene as the electron transporting layer, LiF as the electron injection layer and Al as the cathode electrode, with the corresponding deposition rates of 1.0, 0.1 and 10.0 Å s⁻¹, respectively. The *J*-*V*-*L* measurements were carried out at room temperature in a nitrogen-filled glovebox. A Keithley 2450 source meter and fibre integration sphere (FOIS-1) coupled with a QE Pro spectrometer (Ocean Optics) were used for the measurements. The OLED devices were tested on top of the integrating sphere, where only forward light emission can be collected. The absolute OLED emission was calibrated by a standard visible-near-infrared light source (HL-3P-INT-CAL plus, Ocean Optics).

Fabrication of OLED devices with stretchable TADF polymer films under stretching

The fabrication and measurement are similar to conventional rigid OLED fabrication, but with the hole injection layer/hole transporting layer and EML using different materials. For the hole injection layer/hole transporting layer, a mixture of PEDOT:PSS solution, PFI solution and IPA at a volume ratio of 1:1:5 were mixed and then spin coated on ITO substrates at 4,500 rpm for 1 min. After that, the device was transferred into a glovebox for the following processes. On top of the PEDOT:PFI surface, a mixed solution of SEBS:mCP (at a 1:1 weight ratio) in CB with 8 mg ml⁻¹ was spin coated at 3,000 rpm for 30 s, followed by annealing of the film at 80 °C for 15 min. The EML layer was separately prepared by spin coating the CB solution of the TADF polymer (8 mg ml⁻¹) on MPTS-Si at 2,000 rpm for 30 s, followed by annealing at 120 °C for 30 min. Then, a piece of PDMS stamp was used to peel off the TADF polymer film, apply a strain between 0 and 100%, and then physically transfer the film onto the SEBS:mCP layer in the device through baking at 85 °C for 5 min. Next, the electron transporting layer, electron injection layer and cathode layer were deposited through thermal evaporation, with the same set of materials and conditions as conventional rigid OLEDs described in the above section.

Characterization of PEDOT:PSS_PFI and PEIE_PFN-Br thin films

The thin films of PEDOT:PSS_PFI were prepared through the spin coating of the mixture solution (PEDOT:PSS solution:PFI solution:IPA = 1:1:3 (v:v:v)) on OTS-modified Si substrates (OTS-Si) at 3,000 rpm for 1 min, and then annealed at 130 °C for 30 min, which yielded a film thickness of around 110 nm. The thin films of PEIE_PFN-Br were prepared through the spin coating of the mixture solution (total of 0.25 wt% in methanol at a weight ratio of 1:1) on OTS-Si at 3,000 rpm for 30 s and annealed at 100 °C for 10 min, which yielded a film thickness of around 20 nm. The films were transferred to PDMS stamps to apply different strains and then transferred to SEBS-coated Si substrates for characterizations. For the XPS test, PEDOT:PSS_PFI composite films were measured from the top surface on OTS-Si substrate and the bottom surface on PDMS substrate (transferred from OTS-Si). For the UPS and Raman tests, the preparations of films were similar, except that O₂-plasma-treated (150 W, 3 min) Si was used as the substrate.

Fabrication of stretchable semitransparent electrodes

The schematic of the fabrication process is described in Supplementary Fig. 34. AgNW solution (AW045, 1 wt% in water) was first vortexed for 10 min to remove big aggregations and then diluted in IPA (1:19 by volume), followed by 10 s bath sonication. Next, the solution was spray coated on a cleaned OTS-Si substrate under 100 °C, until the target sheet resistance of around 3 Ω sq⁻¹ was reached. The pattern was made with Kapton tape masks. After removing the masks, the AgNW on OTS was washed with deionized water to remove the surfactant, and then dried at 110 °C for 5 min. Next, a TPU solution (20 mg ml⁻¹ in tetrahydrofuran (THF)) was spin coated onto AgNW at 3,000 rpm for 30 s. After drying at 110 °C for 20 min, AgNW covered by TPU was treated with O₂ plasma (150 W) for 1 min. Then, the PDMS mixture (base:crosslinker

ratio of 15:1) was drop casted onto TPU and subsequently degassed under a vacuum and cured at 80 °C for 4 h. After the delamination from the OTS-Si substrate, the AgNW_TPU/PDMS electrode was ready to be used for the fabrication of fully stretchable OLEDs.

Fabrication of fully stretchable OLED devices

The schematic of the fabrication process is described in Supplementary Fig. 39. The separately prepared AgNW_TPU/PDMS electrode was laminated on an OTS-treated glass substrate (OTS-glass) with the AgNW side facing up, and then treated with O₂ plasma (150 W) for 10 s. The PEDOT:PSS_PFI mixture solution in IPA (PEDOT:PSS:PFI = 1:1:3 (v:v:v)) was spin coated at 3,000 rpm for 1 min and then annealed at 130 °C for 30 min, which yielded a film with a thickness of 110 nm. Then, a PDKCD solution (8 mg ml⁻¹ in CB) was spin coated at 1,000 rpm for 30 s and annealed at 120 °C for 30 min, resulting in a 50 nm film. Next, PEIE_PFN-Br solution (total 0.25 wt% in methanol at a weight ratio of 1:1) was spin coated at 3,000 rpm for 30 s and annealed at 100 °C for 10 min, resulting in a 20 nm film. Afterwards, the samples were released from OTS-glass. Another piece of the AgNW_TPU/PDMS electrode was gently laminated on the top and it served as the cathode. Finally, the device was heated at 80 °C for 5 min to enhance adhesion among the layers. The performed measurements are the same as the rigid devices.

Data availability

The data that support the findings of this study are available within this Article and its Supplementary Information. Additional data are available from the corresponding authors upon request. Source data are provided with this paper.

Code availability

The codes and force-field parameters used for the MD simulation are available via GitHub at <https://github.com/czhangR/High-efficiency-stretchable-light-emitting-polymers-from-thermally-activated-delayed-fluorescence.git>. The Gaussian (<https://gaussian.com/>) package is commercially available; the LAMMPS (<https://www.lammps.org/#gsc.tab=0>) and GROMACS (<https://www.gromacs.org/>) packages are open-source.

References

- Li, Q. et al. Through-space charge-transfer polynorbornenes with fixed and controllable spatial alignment of donor and acceptor for high-efficiency blue thermally activated delayed fluorescence. *Angew. Chem. Int. Ed.* **59**, 20174–20182 (2020).
- Shao, S. et al. Blue thermally activated delayed fluorescence polymers with nonconjugated backbone and through-space charge transfer effect. *J. Am. Chem. Soc.* **139**, 17739–17742 (2017).
- Frisch, M. J. et al. Gaussian 09 Revision B.01 (Wallingford CT, 2016).
- Abraham, M. J. et al. GROMACS: high performance molecular simulations through multi-level parallelism from laptops to supercomputers. *SoftwareX* **1–2**, 19–25 (2015).
- Plimpton, S. Fast parallel algorithms for short-range molecular dynamics. *J. Comput. Phys.* **117**, 1–19 (1995).
- Stukowski, A. Visualization and analysis of atomistic simulation data with OVITO—the open visualization tool. *Model. Simul. Mat. Sci. Eng.* **18**, 015012 (2010).
- Hanwell, M. D. et al. Avogadro: an advanced semantic chemical editor, visualization, and analysis platform. *J. Cheminform.* **4**, 17 (2012).
- Martinez, L., Andrade, R., Birgin, E. G. & Martinez, J. M. PACKMOL: a package for building initial configurations for molecular dynamics simulations. *J. Comput. Chem.* **30**, 2157–2164 (2009).
- Martinez, J. M. & Martinez, L. Packing optimization for automated generation of complex system's initial configurations for molecular dynamics and docking. *J. Comput. Chem.* **24**, 819–825 (2003).

60. Chortos, A. et al. Highly stretchable transistors using a microcracked organic semiconductor. *Adv. Mater.* **26**, 4253–4259 (2014).

Acknowledgements

This research is supported by the Start-Up Funds from the University of Chicago, National Science Foundation CAREER Award no. 2239618, and the University of Chicago Materials Research Science and Engineering Center, which is funded by the National Science Foundation under award no. DMR-2011854. We acknowledge the Research Computing Center of the University of Chicago for computational resources. We used the Center for Nanoscale Materials, an Office of Science user facility supported by the US Department of Energy, Office of Science, Office of Basic Energy Sciences, under contract no. DE-AC02-06CH11357. D.V.T. and J.J.d.P. acknowledge support from MICCoM, as part of the Computational Materials Sciences Program funded by the US Department of Energy, Office of Science, Basic Energy Sciences, Materials Sciences and Engineering Division, under grant DOE/BES 5J-30161-0010A. D.V.T. acknowledges support from the National Science Foundation under grant no. DMR-2019444. R.A. is supported by the Dutch Research Council (NWO Rubicon 019.202EN.028). X.Z. acknowledges support from the National Natural Science Foundation of China under grant no. 51821002. We thank X. M. Lin for assisting us with the experiment at Argonne National Laboratory. We thank M. Zhang, X. K. Liu, X. D. Ma, P. J. Pei, C. Arneson and S. R. Forrest for helping with the experiments, and D. F. Yuan and L. P. Yu for discussions about polymer synthesis.

Author contributions

S. Wang. conceived the research. W.L. and S. Wang. designed the experiments. W.L. synthesized the stretchable TADF polymers, fabricated the rigid and fully stretchable OLEDs, and performed the

characteristics and measurements. C.Z., R.A., H.L. and J.J.d.P. performed the simulation. C.Z., Y. Li. and Y. Liu. helped with the film transfer process and fully stretchable device fabrication. X.F., K.W., H.C. and D.V.T. helped with the OLED performance characterization. B.T.D. performed the PL transient decay measurement. C.Z. carried out the PLQY measurement. X.F. and K.W. measured the low-temperature FL/PH spectra. Q.L., S.S. and L.W. provided the PNB-TAc-TRZ-5 and P-Ac95-TRZ05 polymers. S. Wang. and J.J.d.P. supervised the research. W.L., C.Z., S. Wang. and J.J.d.P. wrote the manuscript. All the authors contributed to the discussion and manuscript revision.

Competing interests

S.W., J.J.d.P., W.L. and C.Z. are inventors on a pending patent filed by the University of Chicago (no. UCHI 22-T-048). The other authors declare no competing interests.

Additional information

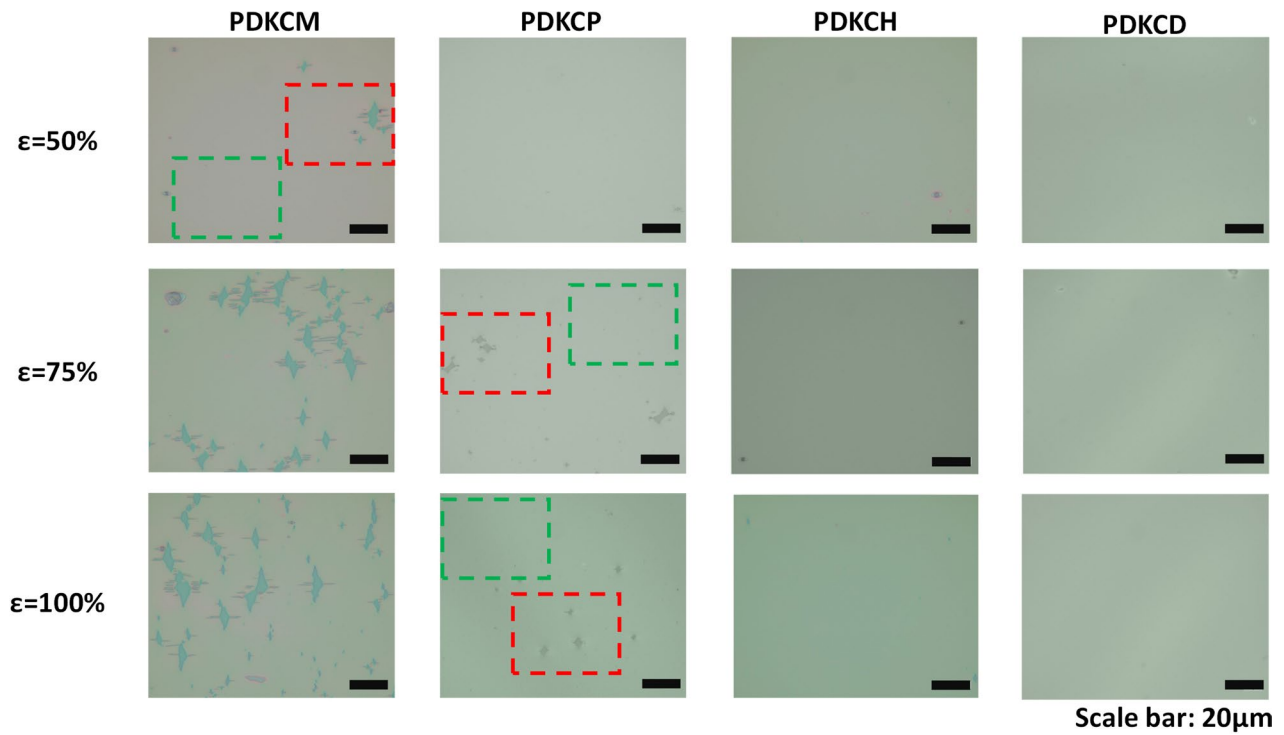
Extended data is available for this paper at <https://doi.org/10.1038/s41563-023-01529-w>.

Supplementary information The online version contains supplementary material available at <https://doi.org/10.1038/s41563-023-01529-w>.

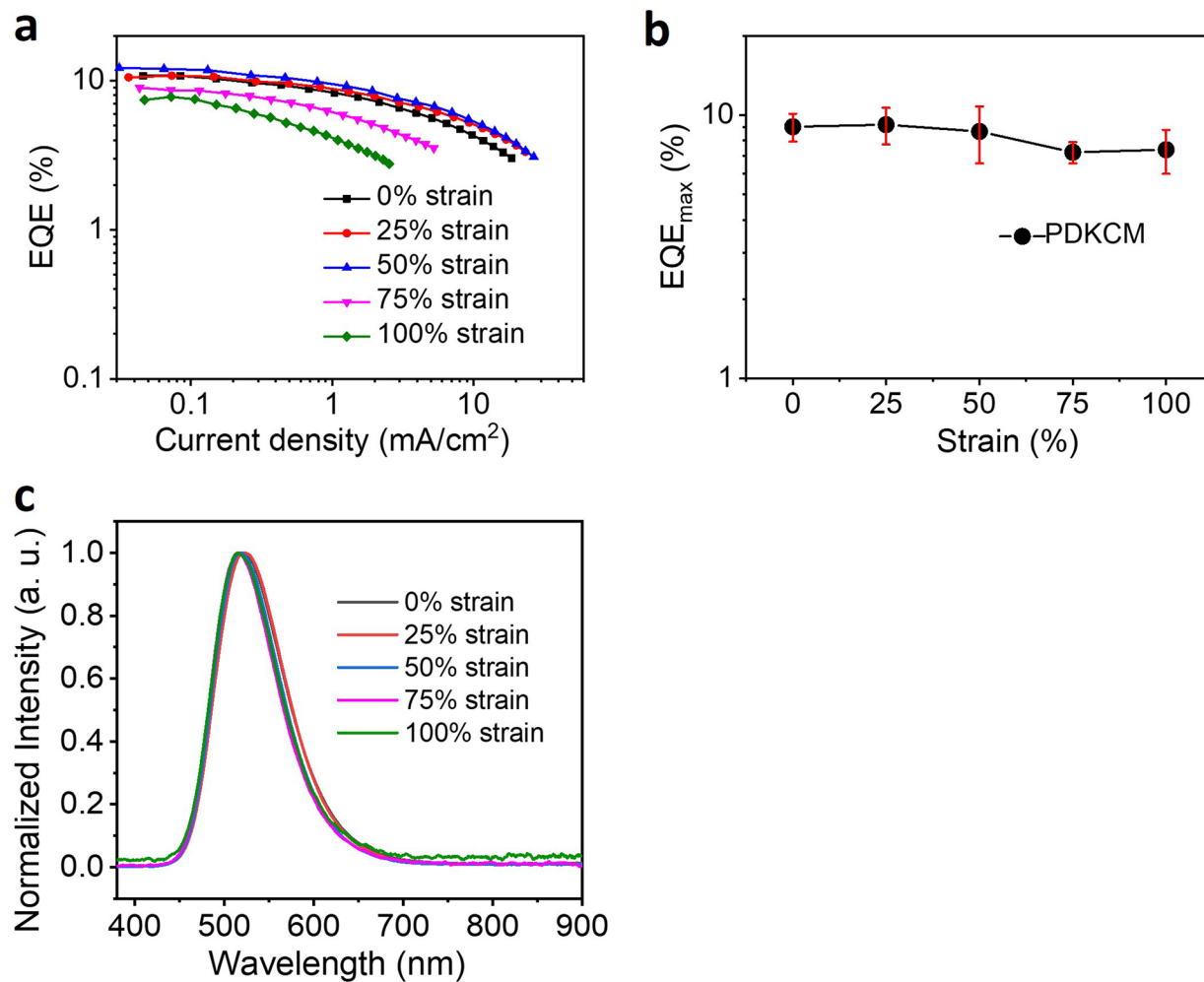
Correspondence and requests for materials should be addressed to Juan J. de Pablo or Sihong Wang.

Peer review information *Nature Materials* thanks Tsuyoshi Sekitani and the other, anonymous, reviewer(s) for their contribution to the peer review of this work.

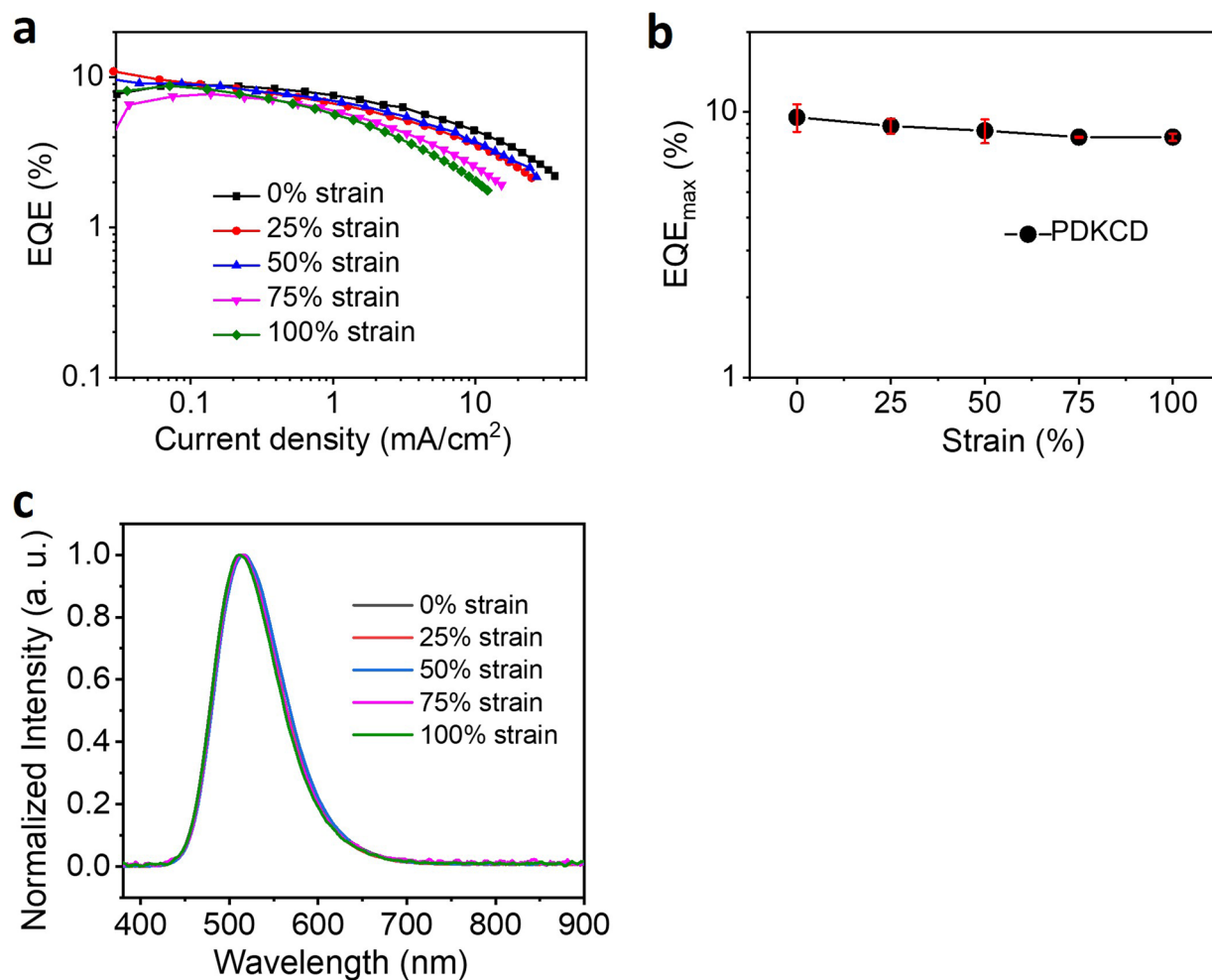
Reprints and permissions information is available at www.nature.com/reprints.



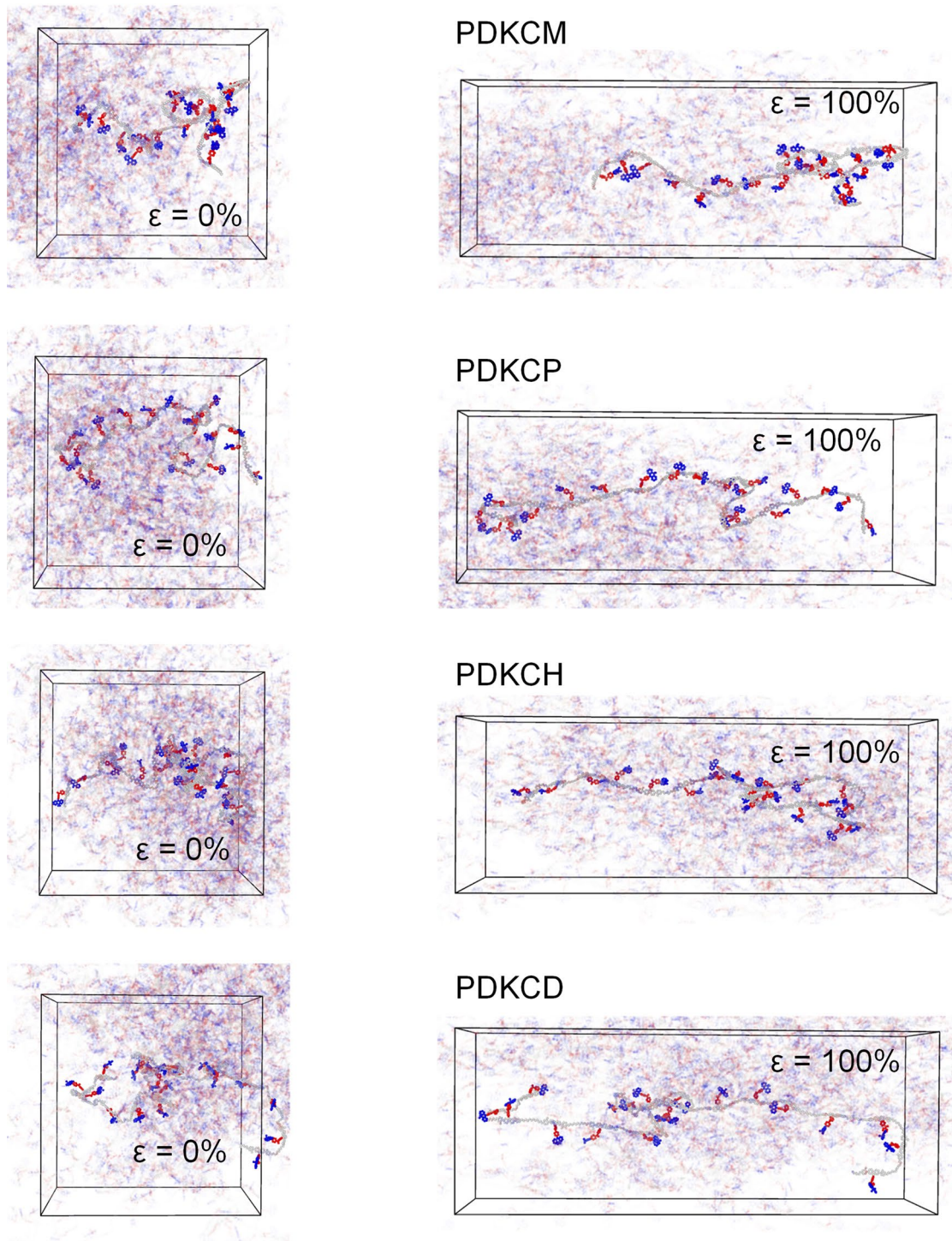
Extended Data Fig. 1 | Optical microscopy images of PDKCM, PDKCP, PDKCH, and PDKCD films under stretching to the strains of 50%, 75%, and 100%. The films were transferred from PDMS substrates to SEBS-coated Si substrates. The stretching direction was horizontal.



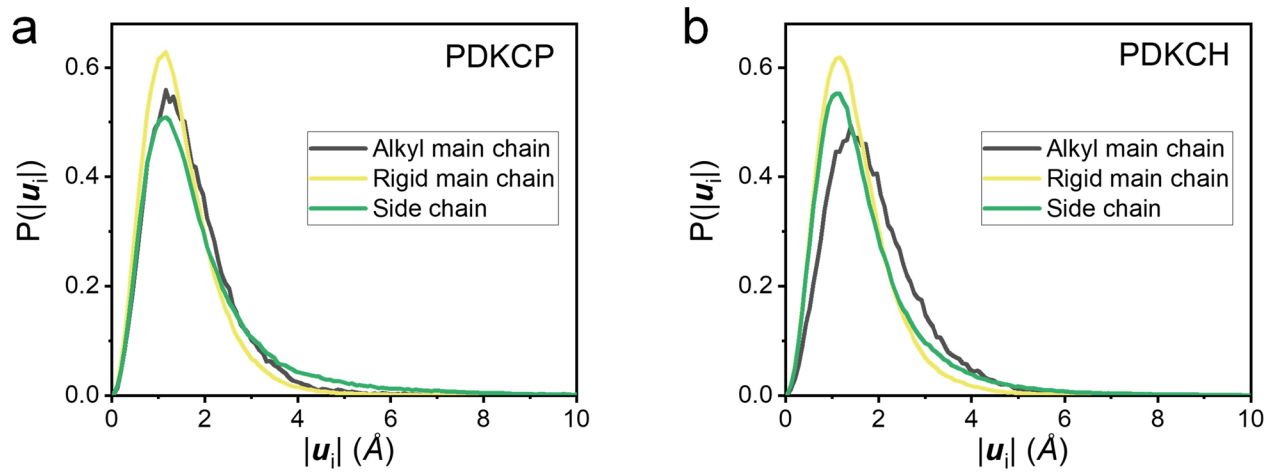
Extended Data Fig. 2 | EL performance of the rigid OLED devices with PDKCM as the emitting layer under different strains. (a) Representative EQE-current density plots. **(b)** Averaged maximum EQE (EQE_{max}) values as a function of different strains. The data of EQE are represented as mean values \pm s.d. from 3 devices. **(c)** Representative EL spectra at 8 V.



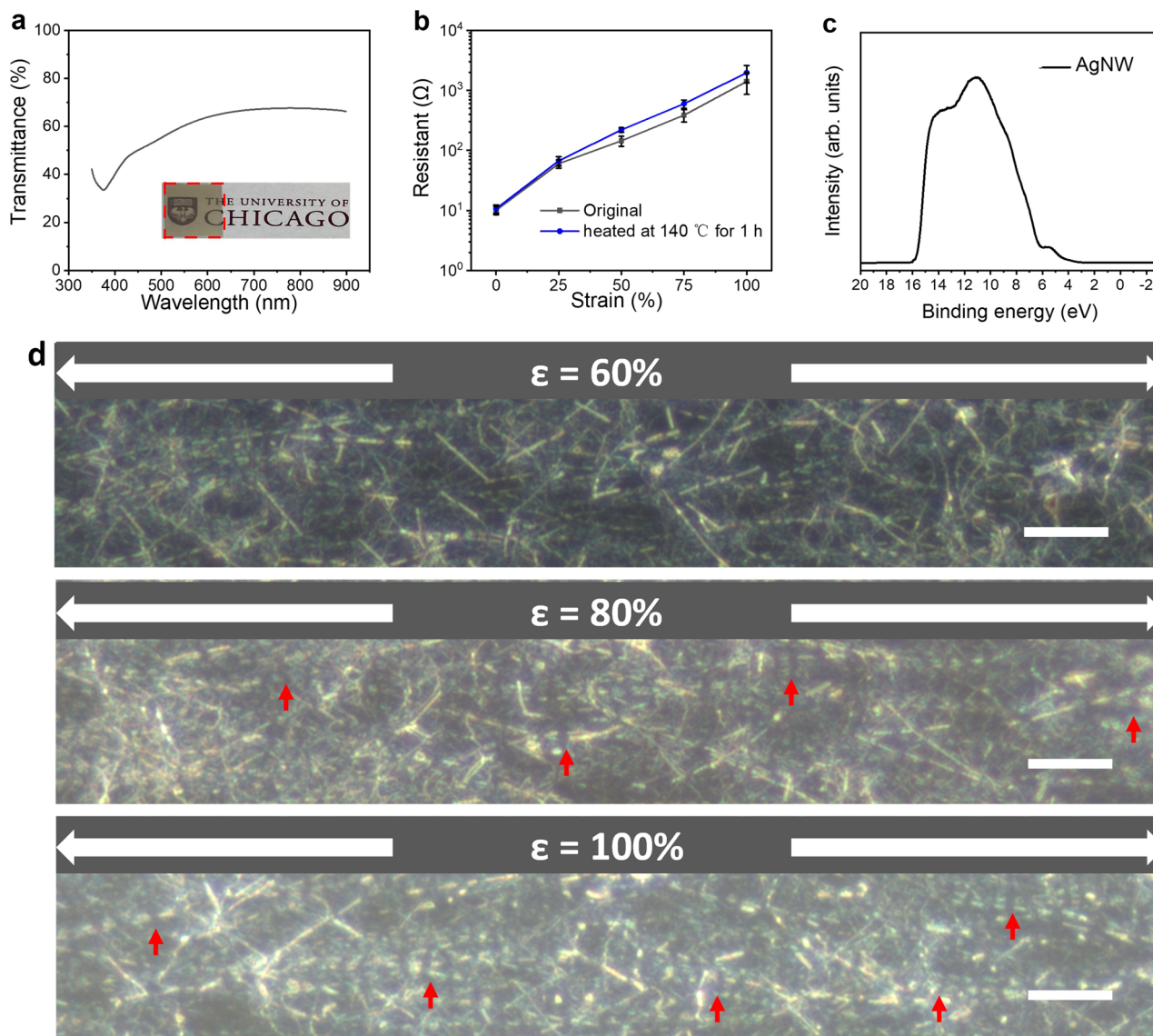
Extended Data Fig. 3 | EL performance of the rigid OLED devices with PDKCD as the emitting layer under different strains. (a) Representative EQE-current density plots. **(b)** Averaged EQE_{max} values as a function of different strains. The data of EQE are represented as mean values \pm s.d. from 3 devices. **(c)** Representative EL spectra at 8 V.



Extended Data Fig. 4 | Snapshots taken from the MD simulations of PDKCM, PDKCP, and PDKCH at 0% and 100% strains. One randomly selected chain is highlighted for each simulation and manually centred at the middle of the box, with the backbone rendered in grey, the electron-donor units in blue, and the electron-acceptor units in red.

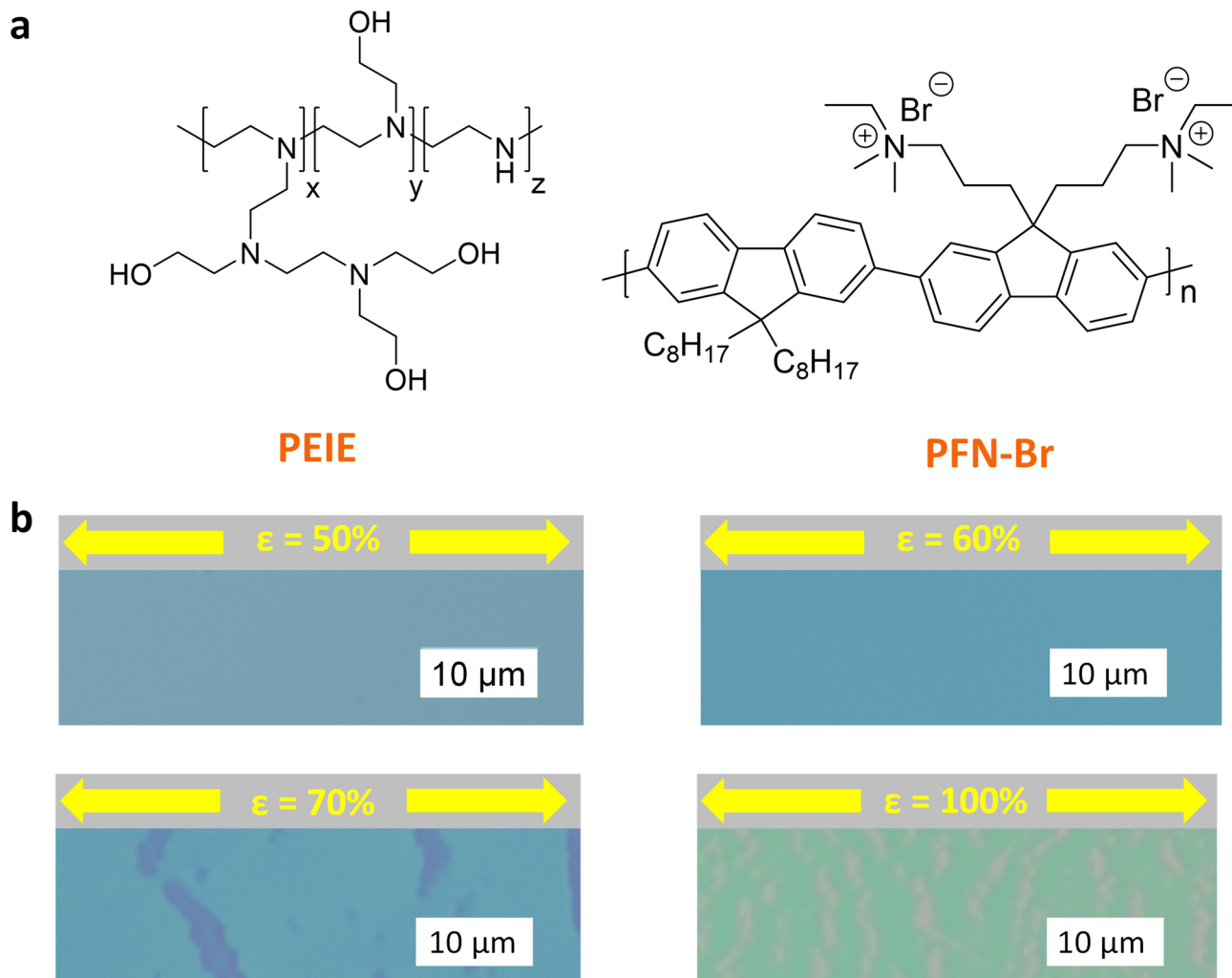


Extended Data Fig. 5 | Non-affine displacements for PDKCP and PDKCH in MD simulations. The non-affine displacements of the alkyl main chain, rigid main chain, and side chain at 5% strain for polymers PDKCP (a) and PDKCH (b).

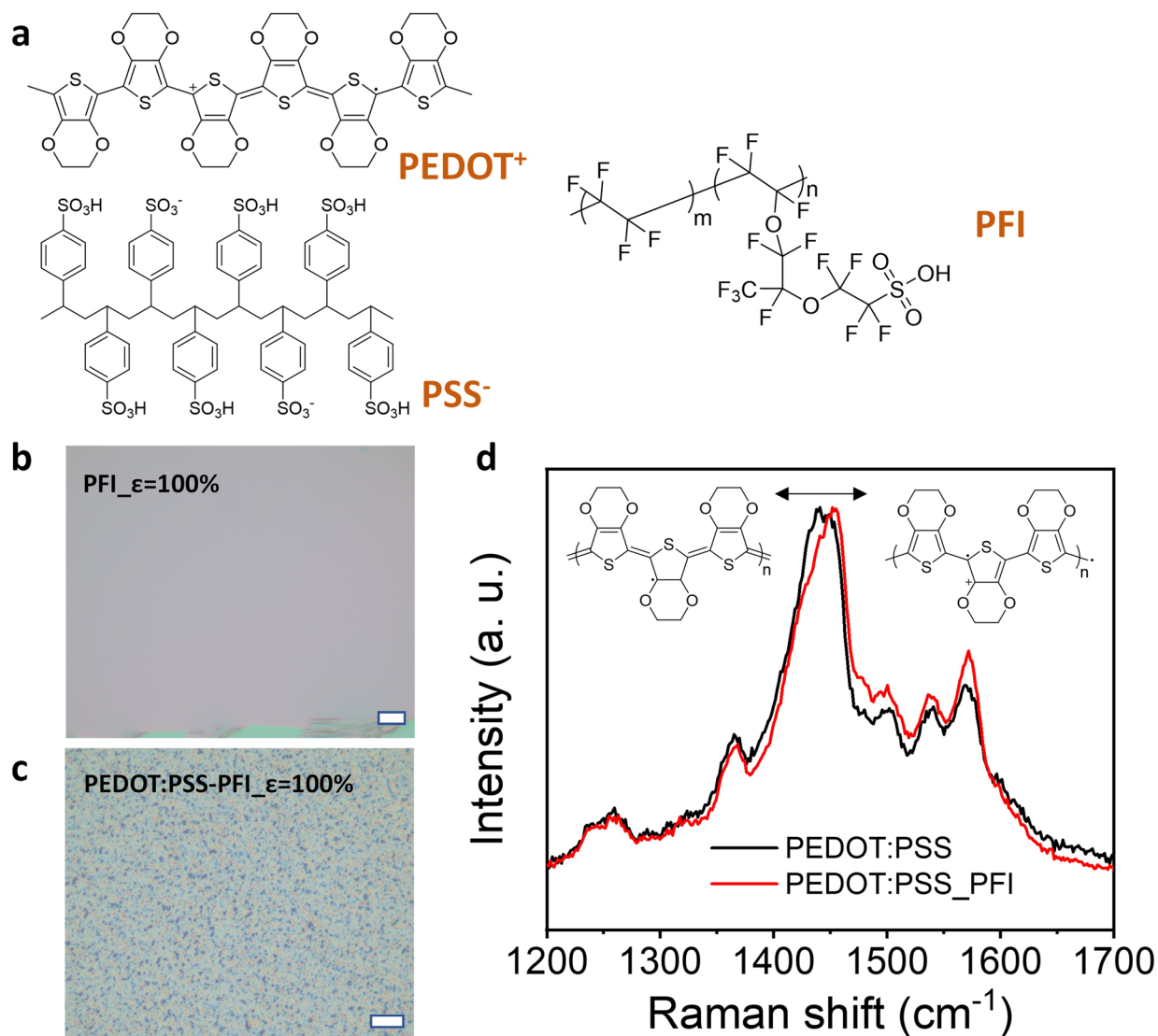


Extended Data Fig. 6 | Characterization of the AgNW/TPU/PDMS electrode. (a) Transmittance curve of the electrode. The inset is the photo of the electrode. (b) Stretching-induced resistance changes for the original electrode and the annealed electrode (140 °C for 1 h). The data of the resistance are represented as mean values \pm s.d. from 5 samples. (c) UPS test result of the electrode. The

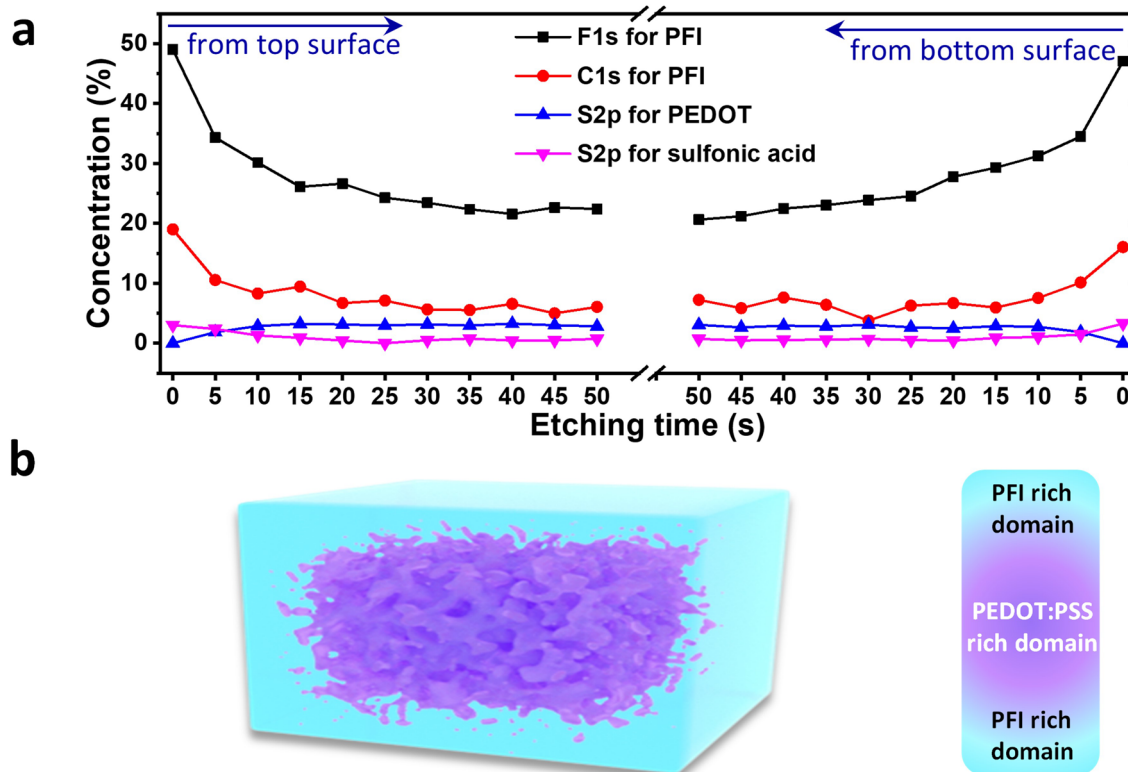
work function (E_{WF}) of the electrode was calculated with the equation: $E_{WF} = h\nu - E_{SE} = 21.22 \text{ eV} - 16.48 \text{ eV} = 4.74 \text{ eV}$, where $h\nu$ is the incident photon energy, ESE is the secondary edge position. (d) Optical microscopy image of the electrode under different strains (60%, 80%, and 100%). The stretching direction is horizontal. The Scale bars are 10 μm .



Extended Data Fig. 7 | Stretchability test of PEIE/PFN-Br composite film. (a) The chemical structures of PEIE and PFN-Br. (b) Optical microscopy images of PEIE/PFN-Br composite films at 50%, 60%, 70%, and 100% strains. The stretching direction is horizontal. Therefore, the composite film can be stretched to 60% without cracking.



Extended Data Fig. 8 | Characterization of the PEDOT:PSS_PFI composite film. (a) Chemical structures of PEDOT:PSS and PFI. (b and c) Optical microscopy images of PFI (b), and PEDOT:PSS_PFI composite film (c), under 100% strain. The stretching direction is horizontal, and the scale bar is 10 μm . (d) Raman spectra of PEDOT:PSS and PEDOT:PSS_PFI film under 632.8 nm laser excitation.



Extended Data Fig. 9 | Vertical phase-separation morphology of the PEDOT:PSS/PFI composite film. (a) Molecular depth (with the step size of ~5 nm) profiles of PEDOT:PSS/PFI composite film as inferred from the XPS results in Supplementary Figs. 36 and 37. Deconvoluted S 2p peaks for PEDOT (164.5 eV), sulfonic acid (S 2p peaks at 168.4 and 168.9 eV), C 1s peak at 291.6 eV, and F 1s peak

for the PFI concentration were used. This shows that the PFI is rich at both top and bottom surfaces in the composite film, and the molecular concentration of PFI gradually decreased toward the centre in the thickness direction. (b) Proposed 3D illustration of the morphology of the PEDOT:PSS/PFI composite film.